Research Square

Preprints are preliminary reports that have not undergone peer review.
They should not be considered conclusive, used to inform clinical practice,
or referenced by the media as validated information.

The glycemic variability induces ovarian dysfunction in NOD mice by inducing ferroptosis

Jiayu Huang
the First Affiliated Hospital of Chongqing Medical University
An He
the First Affiliated Hospital of Chongqing Medical University
Ying Chen
Shanghai First Maternity and Infant Hospital
Yin Tian
Women and Children's Hospital of Chongqing Medical University
Xinmiao Tan
Women and Children's Hospital of Chongqing Medical University
Yingyu Tian
Women and Children's Hospital of Chongqing Medical University
Hanke Zhang
Huazhong University of Science and Technology
Jiying Hou
houjiying@hotmail.com

Chongqing Medical and Pharmaceutical College
Shimeng Guo
Women and Children's Hospital of Chongqing Medical University

Research Article

Keywords:

Posted Date: September 1st, 2026

DOI: https://doi.org/10.21203/rs.3.rs-10557220/v1

License: This work is licensed under a Creative Commons Attribution 4.0 International License.
Read Full License

Additional Declarations: No competing interests reported.

Abstract

Background

As the onset of diabetes shifts toward younger populations, a substantial number of women of reproductive age are affected by dysregulated glycemia. During diabetes management, the degree of fluctuation blood glucose levels in individual over a specific period is defined as glycemic variability, which is closely associated with the risk of diabetic complications. We discuss the relationship between glycemic variability and ovarian function.

Results

We established a recurrent hypoglycemia model using Non-Obese Diabetic (NOD) mice. The mice experienced blood glucose fluctuations showed significantly reduced ovarian volume, diminished the number of healthy antral follicles, and lowered serum Anti-Müllerian Hormone (AMH) levels. A step further, transcriptomic analysis revealed that lipid metabolism and ferroptosis were closely correlated with follicular atresia. Protein-protein interaction (PPI) networks point to ferroptosis as a pathological mechanism. We compared this to traditional biomarkers of apoptosis, while no significant changes were observed in apoptosis-related markers (Bax, Bcl-2, and Cleaved Caspase-3). The hypoglycemia showed lipid peroxidation and oxidative stress in ovarian tissues, as elevated levels of malondialdehyde (MDA) and reactive oxygen species (ROS). Concurrently, it downregulated the expression of ferroptosis inhibitors (glutathione peroxidase 4 (GPX4) and ferritin) and upregulated the key ferroptosis executor acyl-CoA synthetase long-chain family member 4 (ACSL4). These findings suggested that follicular atresia is mediated by ferroptosis rather than classical apoptosis. In vitro experiments further verified that the human ovarian granulosa cell line KGN exhibited typical ferroptotic characteristics after glycemic fluctuation simulation, including mitochondrial structural abnormalities, lipid droplet accumulation, and enhanced oxidative stress. Notably, these molecular and morphological alterations were effectively reversed by the ferroptosis inhibitor Liproxstatin-1.

Conclusion

Our findings demonstrate that recurrent hypoglycemia could induce oxidative stress, disrupts lipid metabolism, and ultimately activates the ferroptosis pathway, thereby causing ovarian granulosa cell damage and follicle loss.

Introduction

Diabetes mellitus (DM) represents a major global public health challenge, with pathological consequences extending far beyond metabolic dysregulation to include multi-organ damage[1–3]. Among the various systemic complications, reproductive dysfunction—particularly ovarian insufficiency

and impaired oogenesis—has drawn increasing attention due to its severe impact on fertility and quality of life in women with DM[4]. Notably, while hypoglycemia has been well documented to adversely affect organs such as the heart, brain, and kidneys, its specific impact on ovarian function remains strikingly understudied[1, 5]. To date, no systematic investigation has examined how hypoglycemia contributes to follicular atresia and oogenic impairment, leaving a significant gap in our understanding of diabetic ovarian injury.

Recent advances in cell death mechanisms have highlighted ferroptosis, an iron-dependent form of regulated cell death driven by lipid peroxidation and redox imbalance, as a key contributor to tissue damage in diabetic complications such as cardiomyopathy and nephropathy[6–8]. Key regulators of ferroptosis include glutathione peroxidase 4 (GPX4), the cystine/glutamate transporter SLC7A11, and acyl-CoA synthetase long-chain family member 4 (ACSL4)[9]. However, whether ferroptosis is activated in the ovary under conditions of glucose fluctuation, and whether it serves as a mechanistic link between recurrent hypoglycemia and ovarian dysfunction, has never been explored[10].

Therefore, in this study, we aimed to investigate the role of ferroptosis in hypoglycemia-associated ovarian damage—a novel and previously unaddressed aspect of diabetic reproductive pathophysiology. Using a NOD mouse model subjected to recurrent hypoglycemia, we performed transcriptomic profiling, histological evaluation, and molecular validation to identify key pathways involved. Complementary in vitro experiments employing the human ovarian granulosa cell line KGN were conducted to simulate glycemic fluctuations and directly examine ferroptosis activation. We hypothesized that recurrent hypoglycemia exacerbates ovarian follicular loss and impairs oogenesis by inducing ferroptosis. Elucidating this mechanism may provide new therapeutic targets to preserve ovarian function and fertility in women with diabetes who experience unstable glycemic control.

Materials and Methods

1. Animals and Recurrent Hypoglycemia Model

All animal procedures were carried out according to the guidelines on the China Animal Protection Law and were approved by the Animal Ethics Committee of Women and Children’s Hospital of Chongqing Medical University (Approval No. 2025006; Chongqing, China). Female Non-Obese Diabetic (NOD) mice were purchased from SPF (Beijing) Biotechnology Co., Ltd. At 10 weeks of age, NOD mice weight 180-220g were used in this study. Spontaneous hyperglycemia was confirmed by fasting blood glucose levels exceeding 16.5 mM. Mice from the acute and recurrent hypoglycaemia groups were subcutaneously (s.c.) injected with insulin (10 units/g; Glargine insulin; Lantus-Solostar, Sanofi-Aventis, Schweiz) after an overnight fast. After insulin injection, blood samples were obtained by tail prick for bloodglucose monitoring every 30 min. Hypoglycaemia was considered when the glycemic index was < 3.9 mmol/L[11]. The therapeutic option for mice in the diabetic and control group was identical to the hypoglycaemia groups, except for injection of an equal volume of PBS instead of insulin (Fig. 1A) [12].

2. Histological Analysis and Follicle Quantification

Ovarian tissues fixed in 4% paraformaldehyde were dehydrated through graded ethanol series, embedded in paraffin, and serially sectioned at a thickness of 5 μm. Every fifth section was collected to avoid double-counting of follicles and stained with hematoxylin and eosin (H&E) for morphological evaluation. Follicles at different developmental stages—primordial, primary, secondary, antral, and cystic follicles—were systematically counted under a light microscope by two independent investigators blinded to the experimental groups. Follicles were classified as healthy or atretic based on established morphological criteria, including the presence of pyknotic granulosa cells, disorganized granulosa cell layers, and oocyte degeneration. Serum levels of Anti-Müllerian Hormone (AMH), a biomarker of ovarian reserve, were measured using a commercially available enzyme-linked immunosorbent assay (ELISA) kit according to the manufacturer's protocol. All samples were assayed in duplicate, and the absorbance was read at 450 nm using a microplate reader.

3. RNA Extraction, Library Construction, and Transcriptomic Analysis

Total Ribonucleic Acid (RNA) was extracted from ovarian tissues using TRIzol reagent (Invitrogen) following the manufacturer's instructions. RNA purity and integrity were assessed using a NanoDrop spectrophotometer and an Agilent 2100 Bioanalyzer. Only samples with RNA integrity number (RIN) ≥ 8.0 were used for library preparation. Sequencing libraries were constructed using the NEBNext Ultra RNA Library Prep Kit and sequenced on an Illumina NovaSeq 6000 platform to generate 150 bp paired-end reads. Raw sequencing data were filtered to remove low-quality reads and adaptor sequences using fastp software. Clean reads were aligned to the mouse reference genome (GRCm38) using HISAT2, and gene expression levels were quantified as fragments per kilobase of transcript per million mapped reads (FPKM) using StringTie. Differential expression analysis between control and hypoglycemic groups was performed using the DESeq2 package in R, with thresholds set at adjusted p-value < 0.05 and |log2 fold change| > 0.5. Principal component analysis (PCA) and t-distributed stochastic neighbor embedding (t-SNE) were used to visualize global transcriptomic changes. Gene Ontology (GO) enrichment analysis and Kyoto Encyclopedia of Genes and Genomes (KEGG) pathway analysis were conducted using the clusterProfiler package. Protein–protein interaction (PPI) networks of differentially expressed genes were constructed using the STRING database and visualized in Cytoscape software. The datasets used and/or analysed during the current study are available from the corresponding author on reasonable request.

4. Assessment of Oxidative Stress and Lipid Peroxidation

To evaluate oxidative stress levels in cultured cells. KGN cells were stained with BODIPY™ 581/591 C11 (Thermo Fisher Scientific), a fluorescent probe that shifts from red to green upon oxidation, to detect lipid peroxidation. After staining, cells were washed with PBS, mounted with anti-fade mounting medium containing DAPI, and imaged using a confocal laser scanning microscope. For quantitative analysis, the

ratio of oxidized (green) to reduced (red) fluorescence intensity was calculated using ImageJ software. Additionally, KGN cell lysates were used to measure malondialdehyde (MDA) levels using a thiobarbituric acid reactive substances (TBARS) assay kit according to the manufacturer's protocol. Total reactive oxygen species (ROS) levels were measured using the DCFH-DA fluorescent probe; fluorescence intensity was recorded at excitation/emission wavelengths of 485/535 nm using a fluorescence microplate reader.

5. Immunohistochemistry (IHC) and Immunofluorescence (IF) Staining

For immunohistochemical analysis, paraffin-embedded ovarian sections (5 μm) were deparaffinized in xylene, rehydrated through a graded ethanol series, and subjected to heat-induced antigen retrieval in citrate buffer (pH 6.0). Endogenous peroxidase activity was blocked with 3% hydrogen peroxide, and non-specific binding sites were blocked with 5% normal goat serum. Sections were then incubated overnight at 4°C with primary antibodies against GPX4 (Abcam, 1:200), ACSL4 (Santa Cruz, 1:150), Ferritin (Abcam, 1:300), SLC7A11 (Novus Biologicals, 1:200), Bax (Cell Signaling Technology, 1:250), Bcl-2 (Abcam, 1:250), cleaved Caspase-3 (Cell Signaling Technology, 1:200), and γ-H2AX (Millipore, 1:300). After washing, sections were incubated with horseradish peroxidase (HRP)-conjugated secondary antibodies, developed using 3,3'-diaminobenzidine (DAB) substrate, and counterstained with hematoxylin. Images were captured using a digital slide scanner, and staining intensities were quantified using Image Processing and Analysis in Java (ImageJ).

For immunofluorescence staining, KGN (human ovarian granulosa cell line) was cultured on glass coverslips were fixed with 4% paraformaldehyde, permeabilized with 0.1% Triton X-100, and blocked with 5% bovine serum albumin (BSA). Cells were incubated overnight at 4°C with primary antibodies against GPX4 (1:150) and ACSL4 (1:100), followed by Alexa Fluor-conjugated secondary antibodies (Invitrogen, 1:500). Nuclei were counterstained with 4',6-diamidino-2-phenylindole (DAPI). Coverslips were mounted onto glass slides and imaged using a confocal microscope. Fluorescence intensity was quantified from at least five random fields per group using ImageJ.

6. Cell Culture and In Vitro Hypoglycemic Fluctuation Model

This study used human ovarian granulosa cell line KGN to conducted in vitro cell based experiments.The KGN cell lines were purchased from the China National Collection of Authenticated Cell Cultures. The commercially obtained human cell line was originally established complying with the Declaration of Helsinki with valid ethical approval and donor informed consent. In cell experiments, the KGN cell line was maintained in Dulbecco's Modified Eagle Medium (DMEM) supplemented with 10% fetal bovine serum (FBS), 100 U/mL penicillin, and 100 μg/mL streptomycin at 37°C in a humidified atmosphere containing 5% CO_2. Cells were routinely subcultured every 2–3 days. To simulate glycemic fluctuation in vitro, KGN cells were subjected to alternating cycles of high glucose (25 mM) and low glucose (2.5 mM)

medium supplemented with 100 nM insulin. Each cycle consisted of 1 hour of high glucose followed by 1 hour of low glucose, repeated for a total of 6 cycles. Control cells were maintained in normal glucose medium (11 mM) throughout the experiment. As a positive control for ferroptosis induction, cells were treated with 10 μM Erastin for 24 hours. For rescue experiments, cells were co-treated with 1 μM Liproxstatin-1, a potent ferroptosis inhibitor, during the hypoglycemic fluctuation protocol. At the end of treatments, cells were harvested for RNA and protein extraction, fixed for immunofluorescence, or processed for electron microscopy.

7. Transmission Electron Microscopy (TEM)

KGN cells were fixed in 2.5% glutaraldehyde in 0.1 M phosphate buffer (pH 7.4) for 2 hours at 4°C, post-fixed in 1% osmium tetroxide for 1 hour, and dehydrated through a graded acetone series. Samples were embedded in epoxy resin and polymerized at 60°C for 48 hours. Ultrathin sections (70 nm) were cut using an ultramicrotome, collected on copper grids, and stained with 2% uranyl acetate and lead citrate. Sections were examined under a transmission electron microscope operating at 80 kV. Images were captured at various magnifications to assess mitochondrial morphology, including cristae structure, membrane density, and the presence of vacuoles, as well as intracellular lipid droplet accumulation.

8. Western Blot Analysis

8. Western Blot Analysis
Total protein was extracted from ovarian tissues or KGN cells using Radioimmunoprecipitation assay (RIPA) lysis buffer supplemented with protease and phosphatase inhibitor cocktails. Protein concentrations were determined using the BCA protein assay kit. Equal amounts of protein (20–30 μg) were separated by Sodium Dodecyl Sulfate-Polyacrylamide Gel Electrophoresis (SDS-PAGE) on 10–12% polyacrylamide gels and transferred onto polyvinylidene difluoride (PVDF) membranes. Membranes were blocked with 5% non-fat milk in Tris-buffered saline containing 0.1% Tween-20 (TBST) for 1 hour at room temperature and then incubated overnight at 4°C with primary antibodies against GPX4 (Abcam, 1:1000), ACSL4 (Santa Cruz, 1:500), SLC7A11 (Novus Biologicals, 1:800), and β-actin (Sigma, 1:5000) as a loading control. After washing with TBST, membranes were incubated with HRP-conjugated secondary antibodies for 1 hour at room temperature. Protein bands were visualized using enhanced chemiluminescence (ECL) substrate and detected with a chemiluminescence imaging system. Band intensities were quantified using ImageJ and normalized to β-actin.

9. Animal anesthesia and euthanasia procedures

- At the end of the modeling process (including ovulation-promotion treatment), experimental mice were anesthetized deeply by intraperitoneal injection of 3% pentobarbital at a dosage of 50 mg/kg. Once the mice were completely unconscious (manifested by a decreased respiratory rate and general unresponsiveness), they were placed in a clean, transparent airtight box with ventilation

holes, which was connected to a CO_2 cylinder. First, air was supplied, and then the CO_2 concentration was gradually increased to 100% at a displacement rate of 30%-70% of the container volume per minute. During this process, the mice's responses were closely monitored. When the mice exhibited respiratory or cardiac arrest, it indicated that sufficient CO_2 had been administered. After the mice lost vital signs, death was confirmed by physical methods such as tracheal perforation. Then the ovarian tissues were rapidly dissected. Tissues were either fixed in 4% paraformaldehyde for histological analysis, snap-frozen in liquid nitrogen for molecular studies, or processed for protein and RNA extraction. This procedure complies with the ARRIVE 2.0 guidelines for animal research ethics and adheres to the 3Rs principles of animal welfare to minimize suffering of experimental animals.

10. Statistical Analysis

All quantitative data were expressed as mean ± standard error of the mean (SEM) from at least three independent experiments. Statistical analyses were performed using GraphPad Prism software. Comparisons between two groups were made using two-tailed Student's t-test, while comparisons among multiple groups were analyzed using one-way analysis of variance (ANOVA) followed by Tukey's post hoc test. A p value ≤ 0.05 was considered statistically significant.

Results

1. Repetitive Hypoglycemia Leads to Ovarian Atrophy and Follicular Depletion in NOD Mice

To investigate the impact of acute glycemic fluctuations on ovarian physiology, we established a model of recurrent hypoglycemia in 10-week-old female Non-Obese Diabetic (NOD) mice. (Fig. 1A) The model mice exhibited spontaneous pancreatitis (Fig. 1B) and also exhibiting spontaneous hyperglycemia (fasting blood glucose > 16.5 mM) (Fig. 1D). With repeated induction of hypoglycemia with insulin,gross morphological examination revealed a significant reduction in ovarian size in hypoglycemic mice compared to normoglycemic NOD controls (Fig. 1C). Histological assessment of ovarian sections stained with H&E confirmed a substantial decrease in the total number of follicles across all developmental stages in the hypoglycemic group (Fig. 1F). Further morphometric analysis indicated a distinct alteration in follicular dynamics: the hypoglycemic ovaries exhibited a significant increase in the proportion of cystic follicles and a concurrent decrease in healthy antral follicles (Fig. 1G). Correlating with the diminished ovarian reserve, serum levels of Anti-Müllerian Hormone (AMH), a key marker of ovarian follicular pool, were markedly lower in mice subjected to glycemic instability (Fig. 1H). These findings demonstrate that recurrent hypoglycemia induces significant ovarian dysfunction and follicular loss.

2. Ovarian Transcriptomic Landscape is Profoundly Altered by Hypoglycemic Stress

To elucidate the molecular underpinnings of hypoglycemia-induced ovarian damage, we performed RNA sequencing on ovarian tissues from control and hypoglycemic NOD mice. Differential expression analysis identified 1058 genes with significant alterations (adjusted p value ≤ 0.05, |log2 fold change| ≥0.5) (Fig. 2A), comprising 598 upregulated and 480 downregulated genes in hypoglycemic ovaries (Fig. 2C). Unsupervised dimensionality reduction using t-distributed stochastic neighbor embedding (t-SNE) clearly separated the transcriptomic profiles of the two groups, confirming distinct global gene expression patterns induced by hypoglycemic stress (Fig. 2B).

Gene Ontology (GO) enrichment analysis of the differentially expressed genes (DEGs) highlighted significant involvement in biological processes related to ‘cellular response to oxidative stress’, ‘lipid metabolic process’, ‘apoptotic signaling pathway’, and ‘response to hypoxia’ (Fig. 2E). Concurrently, Kyoto Encyclopedia of Genes and Genomes (KEGG) pathway analysis revealed significant enrichment in pathways such as ‘PPAR signaling pathway’, ‘Hippo signaling pathway’, and ‘Fatty acid metabolism’ (Fig. 2F). Protein–protein interaction (PPI) analysis was performed on the DEGs. KEGG analysis of the top 50 proteins with the highest PPI connectivity indicated that lipid metabolism and ferroptosis are key contributors to ovarian follicular atresia. This transcriptomic signature pointed towards dysregulated lipid metabolism, oxidative stress, and potential engagement of non-apoptotic cell death pathways.

3. Hypoglycemia Triggers Oxidative Stress and Activates the Ferroptosis Pathway in Ovaries

Guided by the transcriptomic data indicating ferroptosis, we directly assessed markers of lipid peroxidation and oxidative stress levels. The fluorescent staining revealed a pronounced increase in oxidized lipids within the hypoglycemic ovaries (Fig. 3A). Consistent with this, biochemical assays confirmed a significant increase in the lipid peroxidation end product MDA and total cellular ROS in ovarian tissues from hypoglycemic mice (Fig. 3B-C). We next examined the expression of key ferroptosis regulators via IHC. Ovaries from hypoglycemic mice exhibited a significant downregulation of GPX4, the primary enzyme that repairs lipid peroxides and a central ferroptosis inhibitor (Fig. 3C).Meanwhile, this phenomenon is most pronounced in ovarian granulosa cells. Ferritin, the major iron storage protein, was also decreased, potentially indicating iron release and contributing to ferroptosis-sensitizing labile iron pools (Fig. 4D). Conversely, the expression of ACSL4, an enzyme that enriches membranes with polyunsaturated fatty acids and is essential for ferroptosis execution, was markedly upregulated (Fig. 4D).. No significant change was observed in the expression of SLC7A11, the catalytic subunit of the cystine/glutamate antiporter, suggesting cell-type or context-specific regulation of this ferroptosis axis.

4. Follicular Atresia in Hypoglycemic Ovaries is not Primarily Mediated by Apoptosis

Given the established link between apoptosis and follicular atresia, we sought to determine its contribution in our model. IHC staining of ovarian sections for key apoptotic markers showed no statistically significant difference in the protein levels of the pro-apoptotic factor Bax, the anti-apoptotic factor Bcl-2, or the activated executioner caspase, cleaved Caspase-3, and gama-H2.X between control and hypoglycemic groups (Fig. 4A-B). Furthermore, the calculated Bax/Bcl-2 ratio, a critical indicator of apoptotic propensity, remained unchanged (Fig. 4C-F). These results collectively suggest that the accelerated follicular atresia observed under conditions of glycemic instability occurs through a cell death mechanism independent of classical apoptosis.

3.5. In Vitro Modeling of Glycemic Fluctuation Induces Ferroptotic Features in Ovarian Granulosa Cells

To establish a direct causal link and explore cell-autonomous effects, we modeled glycemic fluctuation in the human ovarian granulosa cell line, KGN. Consistent with the in vivo findings, cells undergoing the hypoglycemic mimic displayed a significant increase in oxidative stress, as measured by boron-dipyrromethene; 4,4-difluoro-4-bora-3a,4a-diaza-s-indacene (BODIPY) staining, to a level comparable to Erastin-treated positive controls (Fig. 5C). This increase was effectively mitigated by co-treatment with Liproxstatin-1 (Fig. 5C). Transmission electron microscopy (TEM) provided ultrastructural evidence of ferroptosis: both hypoglycemic-mimic and Erastin-treated cells showed characteristic mitochondrial abnormalities, including reduced or vanished cristae, increased mitochondrial membrane density, and the appearance of vacuoles (Fig. 5A). Furthermore, these cells exhibited excessive intracellular lipid droplet accumulation, a hallmark of dysregulated lipid metabolism preceding ferroptosis (Fig. 5B).

At the molecular level, western blot (Fig. 6A-B)and immunofluorescence analyses (Fig. 6C-F) confirmed the ferroptotic signature. KGN cells under hypoglycemic stress showed a significant decrease in GPX4 protein expression and a concomitant increase in ACSL4 expression. The expression of SLC7A11 was slightly decreased but not as dramatically as GPX4. Crucially, all these molecular changes—the downregulation of GPX4, upregulation of ACSL4, and the associated lipid peroxidation—were substantially reversed by the addition of the ferroptosis inhibitor Liproxstatin-1. The rescue experiments with Liproxstatin-1 provide functional validation of the mechanistic role of ferroptosis. The inhibitor not only normalized the expression levels of GPX4 and ACSL4 but also effectively suppressed the accumulation of lipid peroxides (Fig. 5C) and ameliorated mitochondrial damage (Fig. 5A) induced by the hypoglycemic mimic. These results demonstrate that ferroptosis is a major executable pathway through which acute glycemic fluctuation inflicts damage upon ovarian granulosa cells.

Discussion

In mammals, the maintenance of glucose homeostasis is essential for preserving normal physiological functions, and the ovary is particularly sensitive to metabolic perturbations[9, 13]. With the increasing prevalence of diabetes at younger ages, recurrent hypoglycemia has emerged as a critical but underappreciated risk factor affecting women of reproductive age. Although hypoglycemia is widely

recognized for inducing systemic complications, its impact on ovarian function and the underlying molecular mechanisms remain poorly understood[1, 14]. In the present study, we demonstrate that recurrent hypoglycemia induces ovarian dysfunction in NOD mice, characterized by diminished ovarian reserve and accelerated follicular atresia, and further identify ferroptosis as a central mechanism mediating this process .

Our findings indicate that hypoglycemic stress leads to a significant reduction in ovarian volume, a decline in follicle numbers across all developmental stages, and decreased serum AMH levels, collectively reflecting impaired ovarian reserve. These phenotypic alterations are consistent with previous reports showing that metabolic imbalance can disrupt folliculogenesis and endocrine function[15–18]. Transcriptomic analysis further revealed that lipid metabolism and ferroptosis-related pathways are prominently altered under hypoglycemic conditions, suggesting that metabolic stress may converge on redox imbalance and non-apoptotic cell death pathways.

Ferroptosis, a form of regulated cell death driven by iron-dependent lipid peroxidation, has recently been implicated in reproductive disorders [19–24]. In line with this, we observed a marked accumulation of lipid peroxides and oxidative stress in ovarian tissues following hypoglycemia. Notably, the expression of GPX4—a key enzyme responsible for detoxifying lipid peroxides and a central inhibitor of ferroptosis[25–27]—was significantly downregulated, particularly in granulosa cells. Conversely, ACSL4, a critical enzyme that promotes the incorporation of polyunsaturated fatty acids into membrane phospholipids and sensitizes cells to ferroptosis[26, 28], was upregulated. These molecular signatures strongly support the activation of the ferroptotic cascade. Additionally, reduced ferritin levels suggest an increased labile iron pool, which further exacerbates oxidative damage and ferroptosis susceptibility [19].

Interestingly, the expression of SLC7A11/xCT, a key regulator of cystine uptake and glutathione synthesis, remained unchanged in our model[29, 30]. This finding suggests that ferroptosis regulation under hypoglycemic stress may not primarily depend on cystine transport but rather on GPX4 activity and lipid metabolic remodeling. Such context-dependent regulation of ferroptosis has also been reported in other tissues [31], indicating that different metabolic stresses may engage distinct ferroptotic regulatory nodes.

Given that apoptosis is traditionally considered the dominant mechanism of follicular atresia, we further assessed apoptotic markers in ovarian tissues. However, no significant differences were observed between control and hypoglycemic groups, indicating that classical apoptotic pathways are not the primary drivers of follicular loss in this context. This observation reinforces the notion that non-apoptotic cell death pathways, particularly ferroptosis, play a predominant role in hypoglycemia-induced ovarian injury.

To further validate the causal role of ferroptosis, we employed an in vitro model using KGN granulosa cells. Hypoglycemic treatment significantly increased intracellular oxidative stress, which was completely reversed by Liproxstatin-1, a specific ferroptosis inhibitor. These rescue experiments provide direct functional evidence that ferroptosis acts as a key executor of hypoglycemia-induced cellular

damage. Similar protective effects of ferroptosis inhibition have been reported in models of ischemia-reperfusion and metabolic stress[32], further supporting the generalizability of this mechanism.

In addition to ferroptosis, it is important to consider alternative or complementary mechanisms. Hypoglycemia is known to induce mitochondrial dysfunction, endoplasmic reticulum stress, and inflammatory responses [33], all of which may indirectly contribute to ovarian damage[1]. However, the specific molecular signature observed in this study—characterized by GPX4 downregulation, ACSL4 upregulation, and lipid peroxide accumulation—strongly points toward ferroptosis as the dominant pathway. Nevertheless, future studies should explore potential crosstalk between ferroptosis and other stress-response pathways.

Despite these findings, several limitations should be acknowledged. First, the use of an in vivo mouse model may not fully recapitulate the complexity of human ovarian physiology. Second, while our data support a central role for ferroptosis, the upstream metabolic triggers linking hypoglycemia to ferroptotic activation require further investigation. Third, the precise cell-type specificity and temporal dynamics of ferroptosis within ovarian compartments remain unclear. Future studies may provide deeper insights into these mechanisms.

Abbreviations

ACSL4：acyl-CoA synthetase long-chain family member 4;AMH：Anti-Müllerian Hormone; ANOVA：one-way analysis of variance; BSA：bovine serum albumin; DAB：3,3'-diaminobenzidine; DM：Diabetes mellitus; DMEM：Dulbecco’s Modified Eagle Medium;ECL：chemiluminescence; ELISA：enzyme-linked immunosorbent assay; FBS：fetal bovine serum; GPX4：glutathione peroxidase 4; H&E：hematoxylin and eosin; HRP：horseradish peroxidase; ImageJ：Image Processing and Analysis in Java; KGN：human ovarian granulosa cell line; MDA：malondialdehyde; NOD：Non-Obese Diabetic; PBS：phosphate buffered saline; PPI：protein-protein interaction; PVDF：polyvinylidene difluoride; RIPA：Radioimmunoprecipitation assay; ROS：reactive oxygen species; SDS-PAGE：Sodium Dodecyl Sulfate-Polyacrylamide Gel Electrophoresis; SEM：standard error of the mean; TEM：Transmission electron microscopy; TBST：Tris-buffered saline containing 0.1% Tween-20

Declarations

Ethics approval and consent to participate

All animal procedures were carried out according to the guidelines on the China Animal Protection Law and were approved by the Animal Ethics Committee of Women and Children’s Hospital of Chongqing Medical University (Approval No. 2025006; Chongqing, China).

Consent for publication

Not applicable

Availability of data and materials

The datasets generated during the current study are available in the Open Archive for Miscellaneous Data (OMIX) repository of National Genomics Data Center of China, The BioProject number is PRJCA070153, the file number is OMIX018975-01. The web-link: https://ngdc.cncb.ac.cn/omix/view/OMIX018975.

Competing interests

The authors declare that they have no competing interests.

Funding

This work was supported by the National Key R&D Program of China (Grant No. 2023YFC2705400); the National Natural Science Foundation of China（Grant No. 82502008, 82301848）; the Science and Technology Research Program of Chongqing Municipal Education Commission (Grant No. KJQN202500481, KJQN202302813, KJQN202502807).

Authors' contributions

Jiayu huang, Jiying Hou and An He designed the study. Jiying Hou and Ying chen performed the experiments, Jiayu huang wrote the manuscript. Yin Tian and Yinyu Tian analyzed the data, Xinmiao Tan and Hanke Zhang conducted the bioinformatics analysis. Jiayu huang and Shimeng Guo supervised the study. All authors have read and approved the final manuscript.

Acknowledgments

No acknowledgments.

References

1. Karakas, S.E., *Reactive Hypoglycemia: A Trigger for Nutrient-Induced Endocrine and Metabolic Responses in Polycystic Ovary Syndrome.* J Clin Med, 2023. **12**(23).
2. Yapanis, M., et al., *Complications of Diabetes and Metrics of Glycemic Management Derived From Continuous Glucose Monitoring.* J Clin Endocrinol Metab, 2022. **107**(6): p. e2221-e2236.
3. Amiel, S.A., *The consequences of hypoglycaemia.* Diabetologia, 2021. **64**(5): p. 963-970.
4. Tiselko, A.V., et al., *Evaluation of folliculogenesis and oxidative stress parameters in type 1 diabetes mellitus women with different glycemic profiles.* Endocrine, 2024. **85**(3): p. 1131-1140.
5. Muscogiuri, G., et al., *Nutritional guidelines for the management of insulin resistance.* Crit Rev Food Sci Nutr, 2022. **62**(25): p. 6947-6960.
6. Dixon, S.J. and J.A. Olzmann, *The cell biology of ferroptosis.* Nat Rev Mol Cell Biol, 2024. **25**(6): p. 424-442.

7. Li, S., et al., *Ferroptosis at the nexus of metabolism and metabolic diseases.* Theranostics, 2024. **14**(15): p. 5826-5852.
8. Liang, D., A.M. Minikes, and X. Jiang, *Ferroptosis at the intersection of lipid metabolism and cellular signaling.* Mol Cell, 2022. **82**(12): p. 2215-2227.
9. Zhou, Q., et al., *Ferroptosis: mechanisms and therapeutic targets.* MedComm (2020), 2024. **5**(12): p. e70010.
10. Liu, M., K. Wu, and Y. Wu, *The emerging role of ferroptosis in female reproductive disorders.* Biomed Pharmacother, 2023. **166**: p. 115415.
11. Tourkmani, A.M., et al., *Hypoglycemia in Type 2 Diabetes Mellitus patients: A review article.* Diabetes Metab Syndr, 2018. **12**(5): p. 791-794.
12. He, A., et al., *Hypoglycaemia aggravates impaired endothelial-dependent vasodilation in diabetes by suppressing endothelial nitric oxide synthase activity and stimulating inducible nitric oxide synthase expression.* Microvasc Res, 2023. **146**: p. 104468.
13. Wang, Y., et al., *Androgens drive SLC1A5-dependent metabolic reprogramming in polycystic ovary syndrome.* Nat Commun, 2025. **16**(1): p. 7611.
14. Smits, A., et al., *Obese outbred mice only partially benefit from diet normalization or calorie restriction as preconception care interventions to improve metabolic health and oocyte quality.* Hum Reprod, 2022. **37**(12): p. 2867-2884.
15. Dumesic, D.A., et al., *Oocyte environment: follicular fluid and cumulus cells are critical for oocyte health.* Fertil Steril, 2015. **103**(2): p. 303-16.
16. Robker, R.L., J.D. Hennebold, and D.L. Russell, *Coordination of Ovulation and Oocyte Maturation: A Good Egg at the Right Time.* Endocrinology, 2018. **159**(9): p. 3209-3218.
17. Kirillova, A., et al., *The Role of Mitochondria in Oocyte Maturation.* Cells, 2021. **10**(9).
18. Wang, L., et al., *Oxidative stress in oocyte aging and female reproduction.* J Cell Physiol, 2021. **236**(12): p. 7966-7983.
19. Stockwell, B.R., et al., *Ferroptosis: A Regulated Cell Death Nexus Linking Metabolism, Redox Biology, and Disease.* Cell, 2017. **171**(2): p. 273-285.
20. Zhang, D., et al., *Involvement of ferroptosis in the granulosa cells proliferation of PCOS through the circRHBG/miR-515/SLC7A11 axis.* Ann Transl Med, 2021. **9**(16): p. 1348.
21. Wang, F., et al., *BNC1 deficiency-triggered ferroptosis through the NF2-YAP pathway induces primary ovarian insufficiency.* Nat Commun, 2022. **13**(1): p. 5871.
22. Niu, C., et al., *Spermidine suppresses oxidative stress and ferroptosis by Nrf2/HO-1/GPX4 and Akt/FHC/ACSL4 pathway to alleviate ovarian damage.* Life Sci, 2023. **332**: p. 122109.
23. Zeng, W., et al., *Inhibition of ferroptosis counteracts the advanced maternal age-induced oocyte deterioration.* Cell Death Differ, 2025. **32**(6): p. 1071-1085.
24. Ruan, H., et al., *FSP1 regulates ferroptosis and mitochondrial function during mouse oocyte maturation.* Exp Cell Res, 2025. **447**(2): p. 114524.

25. Zhang, W., et al., *GPX4, ferroptosis, and diseases.* Biomed Pharmacother, 2024. **174**: p. 116512.
26. Chen, X., et al., *Ferroptosis: machinery and regulation.* Autophagy, 2021. **17**(9): p. 2054-2081.
27. Liu, Y., et al., *GPX4: The hub of lipid oxidation, ferroptosis, disease and treatment.* Biochim Biophys Acta Rev Cancer, 2023. **1878**(3): p. 188890.
28. Ding, K., et al., *Acyl-CoA synthase ACSL4: an essential target in ferroptosis and fatty acid metabolism.* Chin Med J (Engl), 2023. **136**(21): p. 2521-2537.
29. Koppula, P., L. Zhuang, and B. Gan, *Cystine transporter SLC7A11/xCT in cancer: ferroptosis, nutrient dependency, and cancer therapy.* Protein Cell, 2021. **12**(8): p. 599-620.
30. Chen, S.Y., et al., *NINJ1 regulates ferroptosis via xCT antiporter interaction and CoA modulation.* Cell Death Dis, 2024. **15**(10): p. 755.
31. Jiang, L., et al., *Ferroptosis as a p53-mediated activity during tumour suppression.* Nature, 2015. **520**(7545): p. 57-62.
32. Friedmann Angeli, J.P., S. Miyamoto, and A. Schulze, *Ferroptosis: The Greasy Side of Cell Death.* Chem Res Toxicol, 2019. **32**(3): p. 362-369.
33. Cryer, P.E., S.N. Davis, and H. Shamoon, *Hypoglycemia in diabetes.* Diabetes Care, 2003. **26**(6): p. 1902-12.

Figures

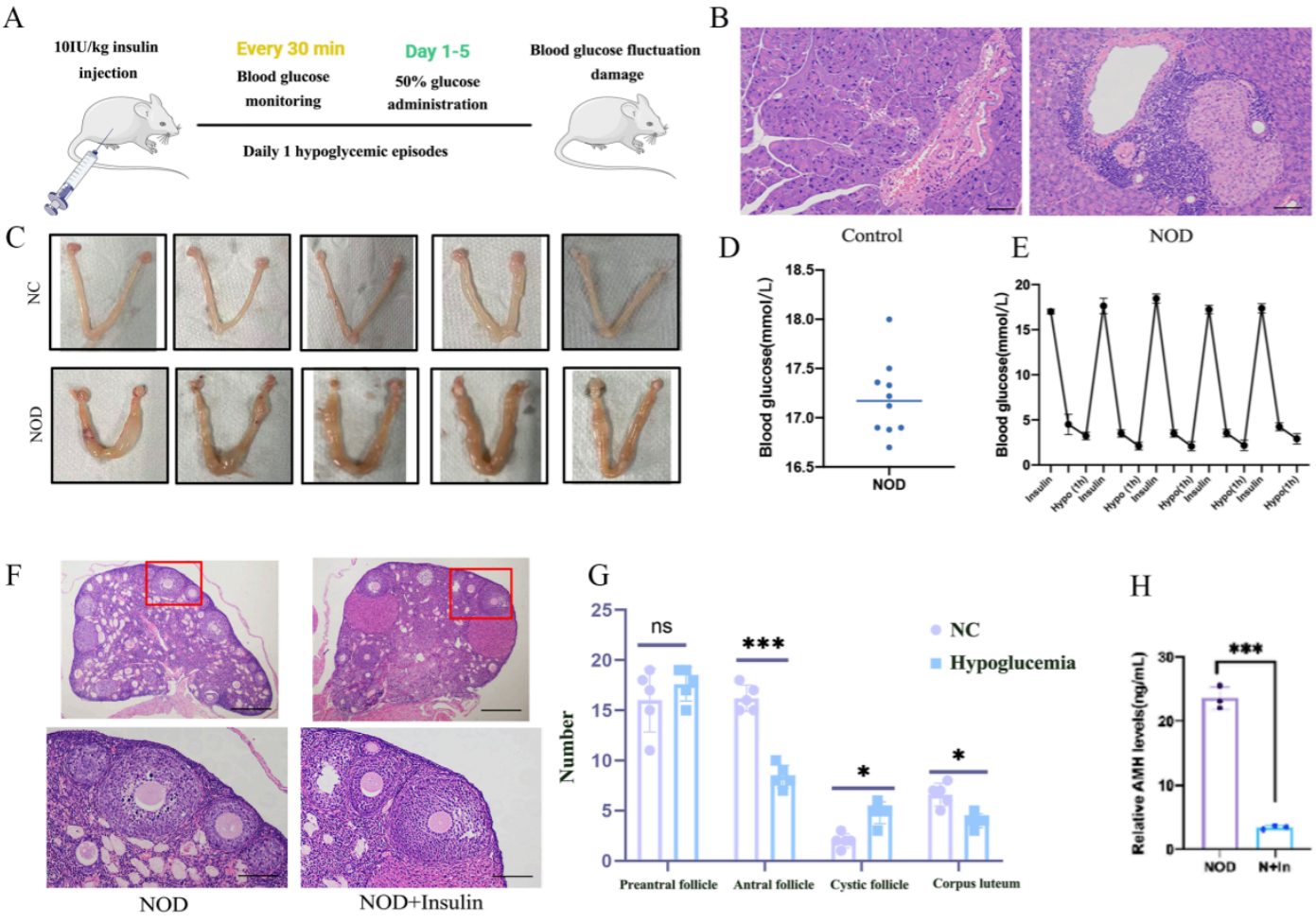


Figure 1

Establishment of the NOD mouse model. A. Schematic of the repeated hypoglycemia mouse model. B. Hematoxylin and eosin (HE) staining of the pancreas in 10-week-old NOD mice.Scale bar: 200μm C. Ovaries and uteri of mice after hypoglycemic challenge. D. Fasting blood glucose levels in 10-week-old NOD mice. E. Insulin-induced blood glucose fluctuations. F. HE-stained ovarian sections of NOD mice. G. Counting of ovarian follicles at different stages in serial sections.Scale bar: 500μm H. AMH levels. Data are means±SEM of at least three independent experiments. *$p < 0.05$, **$p < 0.01$.

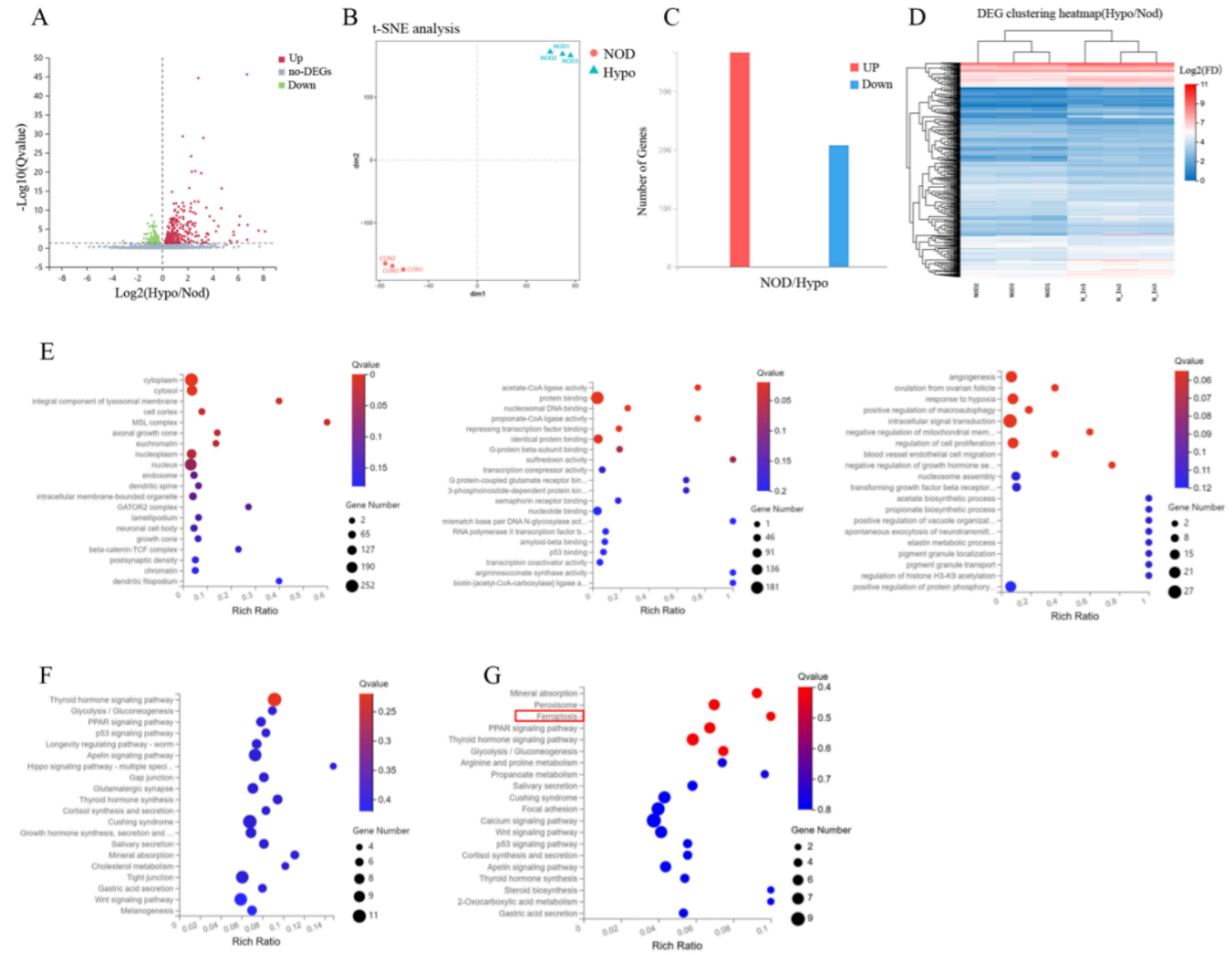


Figure 2

Transcriptomic analysis of ovarian tissues in NOD mice with recurrent hypoglycemia. A. Volcano plot of DEGs. B. t-SNE analysis of transcriptomic profiles. C.The number of DEGs between two groups. D.Heatmap of DEGs. E. GO enrichment analysis of DEGs (biological processes). F. KEGG pathway enrichment analysis of DEGs. G. PPI network of the top 50 proteins with the highest connectivity.

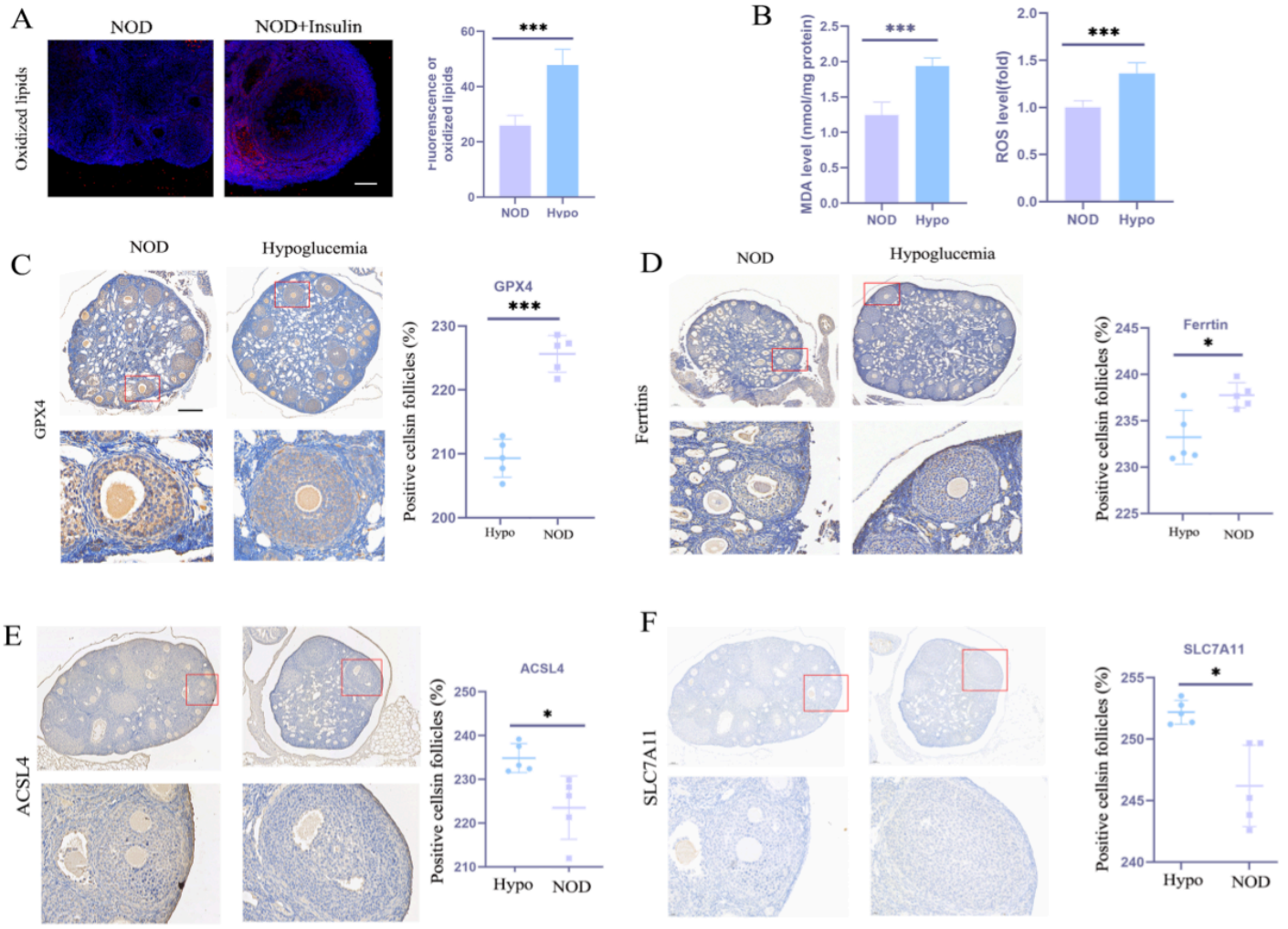


Figure 3

Repeated hypoglycemia induces ferroptosis-related changes in ovarian tissue. A. Ovarian lipid peroxide levels.Scale bar: 100μm B. ROS and MDA levels. C. GPX4 immunohistochemistry and quantitative analysis. D. Ferritins immunohistochemistry and relative expression analysis. E. ACSL4 immunohistochemistry and relative expression analysis. F. SLC7A11 immunohistochemistry and relative expression analysis. Scale bar: 500μm; Data are means±SEM of at least three independent experiments. *$p < 0.05$, **$p < 0.01$.

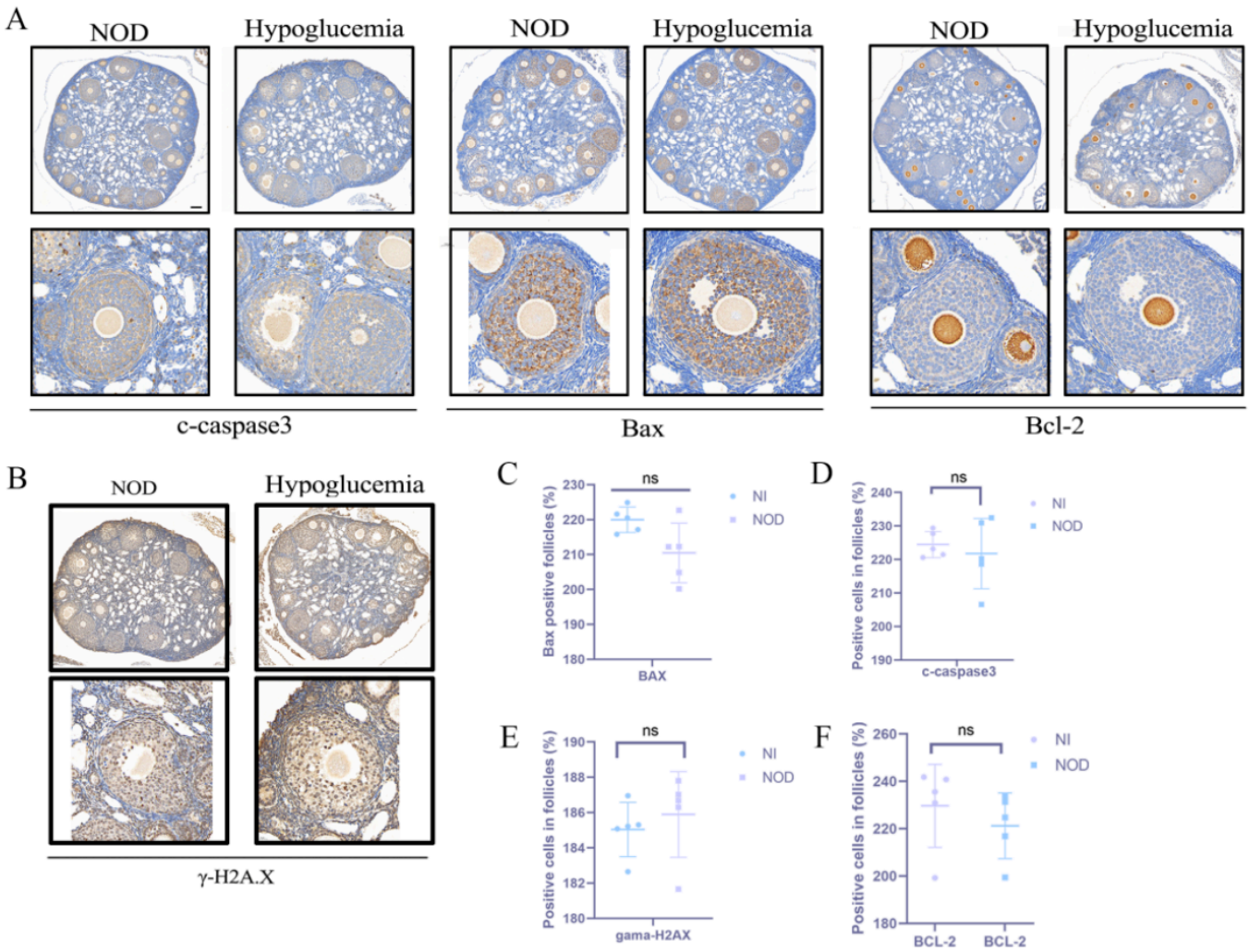


Figure 4

Detection of apoptosis-related proteins. A. Immunohistochemical results of C-caspase3, BAX, and BCL-2. B. Immunohistochemical results of γ-H2A.X. C. Relative quantitative analysis of BAX. D. Relative quantitative analysis of C-caspase3. E. Relative quantitative analysis of γ-H2A.X. F. Relative quantitative analysis of BCL-2. Scale bar: 500μm, Data are means±SEM of at least three independent experiments. ns: no significant difference.

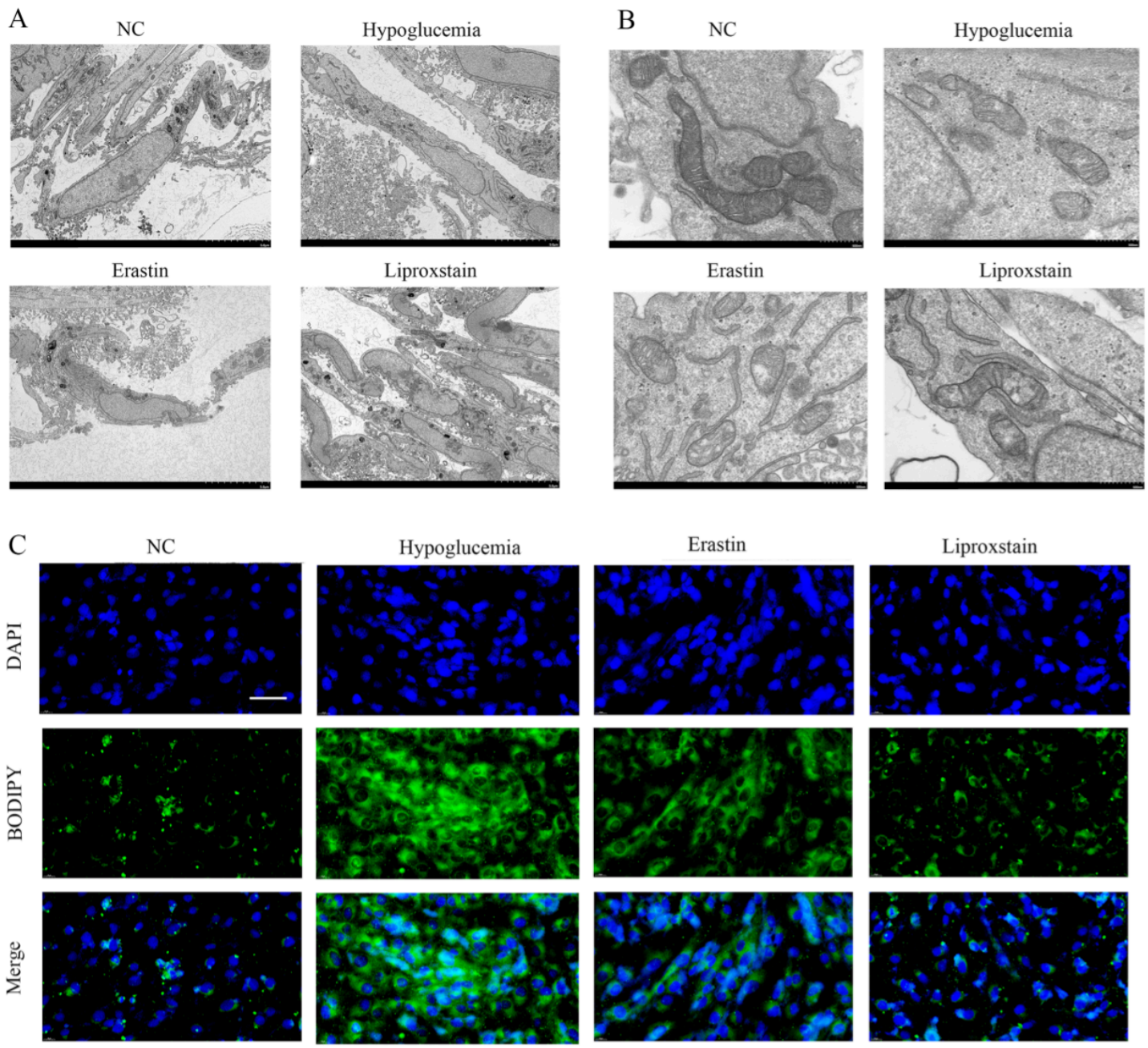


Figure 5

Validation of key ferroptosis markers in vitro. A. Intracellular lipid accumulation observed by electron scanning microscopy, Scale bar: 5μm. B. Mitochondrial morphology in KGN cells under electron microscopy. C. BODIPY staining results of KGN cells; Scale bar: 100μm .

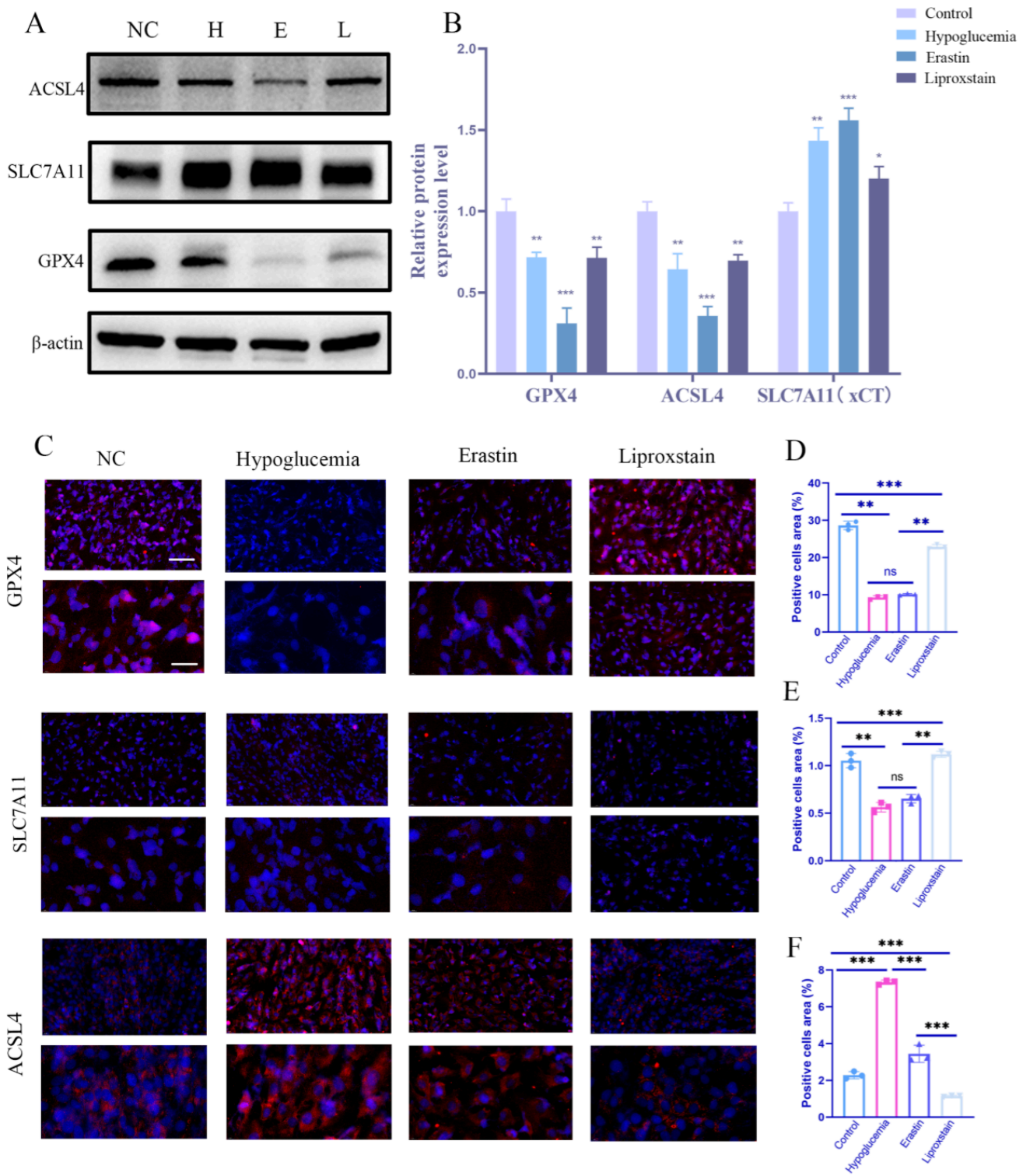


Figure 6

Validation of ferroptosis-related protein expression. A. Western blot analysis of key ferroptosis-related proteins. B. Relative expression level of ACSL4, GPX4 and SLC7A11; C. Immunofluorescence staining of ferroptosis-related proteins. D. Relative expression level of GPX4. E. Relative expression level of XCT. F. Relative expression level of ACSL4. Data are means±SEM of at least three independent experiments. *p < 0.05, **p< 0.01.

Supplementary Files

This is a list of supplementary files associated with this preprint. Click to download.

- Supplementmaterial1.pdf